The Journal of Experimental Biology 212, 155-162
Published by The Company of Biologists 2009
doi:10.1242/jeb.019232

Ultrastructure and physical properties of an adhesive surface, the toe pad epithelium of the tree frog, *Litoria caerulea* White

Ingo Scholz, W. Jon P. Barnes*, Joanna M. Smith† and Werner Baumgartner

Department of Cellular Neurobionics, Institute of Biology 2, RWTH-Aachen, Kopernikusstrasse 16, 52056 Aachen, Germany

*Author for correspondence at present address: Centre for Cell Engineering, Joseph Black Building, Faculty of Biomedical and Life Sciences, University of Glasgow, Glasgow G12 8QQ, UK (e-mail: j.barnes@bio.gla.ac.uk)

†Present address: Biology Teaching Centre, Boyd Orr Building, Institute of Biomedical and Life Sciences, University of Glasgow, Glasgow G12 8QQ, UK

Accepted 10 November 2008

SUMMARY

Knowledge of both surface structure and physical properties such as stiffness and elasticity are essential to understanding any adhesive system. In this study of an adhesion surface in the tree frog, *Litoria caerulea* White, a variety of techniques including atomic force microscopy were used to investigate the microstructure and properties of an epithelium that adheres through wet adhesion. *Litoria* toe pads consist of a hexagonal array of flat-topped epithelial cells, separated by mucus-filled channels. Under an atomic force microscope, this 'flat' surface is highly structured at the nanoscale, consisting of a tightly packed array of columnar nanopillars (described as hemidesmosomes by previous authors), 326±84 nm in diameter, each of which possesses a central dimple 8±4 nm in depth. In fixed tissue (transmission electron microscopy), the nanopillars are approximately as tall as they are broad. At the gross anatomical level, larger toe pads may be subdivided into medial and lateral parts by two large grooves. Although the whole toe pad is soft and easily deformable, the epithelium itself has an effective elastic modulus equivalent to silicon rubber (mean E_{eff}=14.4±20.9 MPa; median E_{eff}=5.7 MPa), as measured by the atomic force microscope in nanoindentation mode. The functions of these structures are discussed in terms of maximising adhesive and frictional forces by conforming closely to surface irregularities at different length scales and maintaining an extremely thin fluid layer between pad and substrate. The biomimetic implications of these findings are reviewed.

Key words: tree frog, adhesion, electron microscopy, atomic force microscopy, effective elastic modulus, tribology.

INTRODUCTION

The study of animal adhesion, for many years a relatively neglected area of research, has recently undergone a resurgence of interest. This is partly because of the promise of practical applications arising from the research – animal adhesive devices have many properties that are the envy of materials scientists – and partly because the application of recent advances in both cell biology and engineering (tribology) has produced a quantum leap forward in our understanding of these systems (Scherge and Gorb, 2001; Barnes, 2006). The reversible adhesion of locomoting animals is of particular interest because of the need to combine good adhesion with easy detachment whenever the animal makes a step (Autumn and Peattie, 2002). Also, in tree frogs, adhesion must not interfere with jumping ability.

Although all tree frogs are not strictly arboreal, for some inhabit the shrub or even herb layer (for instance reeds surrounding ponds), they do all climb vegetation and, along with torrent frogs, are all characterised by possession of expanded digital pads on the tips of each toe. They do not belong to a single systematic group, being found in at least seven different frog families (Duellman and Trueb, 1997). Thus the extraordinary similarity of the epithelia of toe pads in different species is somewhat surprising. Since the main anuran families appeared before the first tree frogs evolved, tree frog toe pads are thus an exceptionally good example of convergent evolution (Green, 1979). There really does appear to be a best 'design' for a toe pad, and this has implications for biomimetics (Barnes, 2007a).

Tree frogs adhere by wet adhesion (Green, 1981; Emerson and Diehl, 1980; Hanna and Barnes, 1991), in the same way as a wet tissue sticks to a flat, smooth surface or a damp coverslip sticks to a microscope slide. The underlying mechanisms are, however, rather more complicated than this simple description would suggest, and involve capillarity forces generated at the air–fluid interface around the edge of the toe pad and transient viscosity forces (Stefan adhesion) generated over the whole area of contact (Barnes et al., 2006b). Current research favours capillarity as the dominant adhesive force (Barnes et al., 2006a), but a role for Stefan adhesion cannot be ignored. Also, friction forces are much larger than would be expected of a fluid joint (Federle et al., 2006). Forces acting parallel to the surface such as friction are clearly the major forces that would prevent slippage while a tree frog was climbing a vertical surface, but recent work (Barnes et al., 2008) also suggests an important role for friction in clinging behaviour on overhanging surfaces. As has recently been hypothesised for geckos (Autumn et al., 2006), frictional forces appear to play a major role in preventing the toe pads from peeling off the surface.

Because adhesion ultimately occurs at the molecular level, its study requires an analysis of both the physical properties of the adhesive surface and its microstructure (Gorb and Scherge, 2000; Scherge and Gorb, 2001). As an example, as any tyre engineer knows, the physical properties of the rubber are just as important as the pattern of the tread. Using the toe pads of White's tree frog (*Litoria caerulea*) as our adhesive surface, this paper brings together a number of anatomical techniques to examine the structure and physical properties of an adhesive epithelium that adheres through wet adhesion. Of particular interest is the use of an atomic force microscope (AFM), the first time this has been used in the study of

tree frog adhesion. In contact imaging mode, it illustrates the structure, in living rather than fixed tissue, of peg-like nanostructures (which we term 'columnar nanopillars') on the 'flat' surfaces of the toe pad epithelial cells. We have also used the AFM as a nanoindenter to measure the stiffness of the toe pad epithelium. What emerges from these studies is that the epithelium of tree frog toe pads is soft (low Young's modulus) and that it has an extremely complex structure, consisting of pillars surrounded by channels at both microscale and nanoscale levels.

MATERIALS AND METHODS

Animals

White's tree frogs (*Litoria caerulea* White, family Hylidae) were purchased from commercial suppliers and maintained in glass vivaria at 20–24°C using heat mats. The vivaria contained foliage, dishes of Cu-free fresh water to maintain a high humidity, branches on which the frogs could climb and sphagnum moss for the frogs to burrow into, all on a gravel base. Frogs were fed on live house crickets dusted with a calcium balancer and multi-vitamin supplement (Nutrobal, purchased from Peregrine Live Foods, Ongar, Essex, UK) twice weekly.

Scanning and transmission electron microscopy

Frogs were killed *via* a lethal dose of benzocaine. Nine toes from each frog, four from the front and five from the back, were fixed in 0.1 mol l^{-1} phosphate-buffered 2.5% glutaraldehyde at pH 7.4 for 24 h. Specimens were then rinsed in phosphate-buffered sucrose, post-fixed in buffered 1% osmium tetroxide for 1 h and washed in distilled water.

For scanning electron microscopy (SEM), specimens were then dehydrated in an acetone series and critical point dried. Samples were mounted and gold-coated before viewing with a Philips SEM 500 scanning electron microscope.

For transmission electron microscopy (TEM), specimens were dehydrated in an alcohol (rather than acetone) series. Samples were rinsed twice in propylene oxide to remove the alcohol, embedded in Spurr's resin and polymerised at 70°C. Ultra-thin sections (60–70 nm) were cut on a Reichert ultramicrotome. These were then mounted on copper grids, stained with uranyl acetate (2% aqueous solution) and lead citrate, and examined using a Philips TEM 301 transmission electron microscope.

Freeze fracture

Freeze fracture was used to examine the inner structure of toe pad epithelial cells, in particular the distribution of cytoskeletal elements. Fresh toes, removed from frogs killed as described above, were plunged into liquid nitrogen at –195°C. The frozen toes were then cracked into a number of pieces using a small piece of a razor blade held in a needle holder, with the aim of getting surfaces that were at right angles to the toe pad epithelial surface. Following freeze drying overnight at –40°C, the specimens were mounted on holders, sputter coated with gold and examined under the SEM.

Atomic force microscopy

To exclude the possibility of artefacts when analysing biological surfaces (such as shrinkage by drying samples for SEM) we made use of atomic force microscopy (AFM). This technique allows measurements to be made directly on the living animal without further treatment of the samples.

AFM was performed on three frogs, previously anaesthetised by immersion in a solution of 0.25 g l^{-1} of benzocaine. This solution was prepared by dissolving 5 g of benzocaine in 100 ml of 95% ethanol, with 5 ml of the resulting solution being diluted in 1 l of distilled water. At this concentration of 0.25 g l^{-1}, prolonged anaesthesia was obtained in about 15 min.

All measurements were carried out in contact mode using a Veeco Dimension III scanning probe microscope (Veeco Digital Instruments, Woodbury, NY, USA) at room temperature. The AFM was equipped with a silicon nitride cantilever with a 4-sided pyramidal shape (Type MLCT, Veeco Instruments), a spring constant of 0.03 N m^{-1} and a centreline-to-face tip angle of 35 deg. (Fig. 1). To avoid disturbance by vibration, the AFM was fixed on elastic bands in an acoustic isolated box.

For the experiments, the frog was laid out ventral side uppermost, with the limb and digit to be studied (largest digit of the hindlimb) fixed to a large glass Petri dish with strips of duct tape. The pad was then completely covered in water to avoid electrostatic or capillary interaction between the tip of the AFM and the sample. All animals recovered after the experiments and were returned to the glass vivarium.

Two types of AFM measurements were carried out: surface imaging of the adhesive toe pads to obtain information on their structure *in vivo*, and indentation experiments to study the mechanical properties of the toe pads.

Imaging the surface of the pad was done by means of surface scans, recording the topography ('height' images) and the cantilever deflection data ('deflection' images). The topography images show the real scales and proportions of the surface parameters, while the deflection images show the bending of the cantilever when it makes contact with the surface during lateral movement. Therefore a deflection image shows the edges and borders of the structure more accurately as it corresponds to a high-pass filtered topography image. General setups and principles for AFM measurements of living biological samples are given in detail by Morris et al. (Morris et al., 1999). The toe pad was scanned under a mechanical impact in the range of 2 to 50 nN. To reduce the possibility of artefacts caused by the mechanical impact of the cantilever, the scanning direction was changed after each scan by 90 deg. Furthermore the angle of the toe was rotated 45 deg. from the axis of the cantilever to ensure that the impact on the cantilever stayed the same although the scanning direction was changed. The scan size was 10 μm×10 μm at a scan rate of 40 μm s^{-1} (2 Hz) for the overview images and

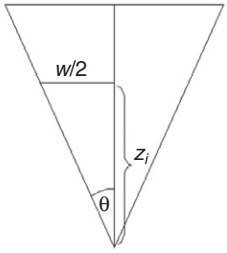

Fig. 1. Vertical section of a 4-sided pyramidal indenter of an atomic force microscope. Calculation of the cross-sectional area of the indenter tip at the indentation depth z_i was as follows:

$$A = w^2,$$

as

$$w/2 = z, \tan\theta,$$

$$A = (2z_i \tan\theta)^2,$$

where w is the width of the AFM indenter tip at the indentation depth and θ equals the tip angle of the indenter (centreline-to-face).

5 μm×5 μm at a scan rate of 40 μm s^{-1} (4 Hz) for the detailed images. To obtain further information on the surface profile parameters, 'sections' within the images were analysed. These sections enabled us to measure the dimensions of the nanopillars.

Measurement of the elastic modulus of the adhesive toe pad was performed with a *z*-drive amplitude of 1600 nm. Multiple measurements were made on three individuals at positions on the pad that varied systematically over the pad surface. Elastic surface properties were investigated by employing force–distance cycles that were recorded at pulling rates of 1 Hz and 2 Hz (3200 nm s^{-1} and 6400 nm s^{-1}). These force–distance cycles were analysed for the determination of the elastic modulus following the theory of Oliver and Pharr (Oliver and Pharr, 2004), who showed that the force–indentation relationship of a flat homogeneous material follows a power law, namely:

$$F = \alpha z_i^m , \quad (1)$$

where F is the applied force, α is a material parameter directly related to Young's modulus, z_i is the indentation depth and m is an exponent representing the geometry of the indenter. As explained in more detail in Scholz et al. (Scholz et al., 2008), $m \approx 2$ for a pyramidal indenter used to indent a soft material. Neither force F nor distance (the indentation depth z_i) is directly accessible. However, force is proportional to cantilever deflection d ($F=kd$), and indentation depth equals the vertical position of the piezo drive z minus the z position where the tip touches the surface z_0 minus the cantilever deflection ($z_i=z-z_0-d$). Eqn 1 thus transforms to:

$$F = kd = \alpha(z - z_0 - d)^2 . \quad (2)$$

Solving Eqn (2) with respect to d gives:

$$d = (z - z_0) + (k/2\alpha) - \sqrt{[(z - z_0) + (k/2\alpha)]^2 - (z - z_0)^2} . \quad (3)$$

Force–distance curves were fitted using this equation, the parameters α and z_0 being optimised by a Levenberg–Marquardt square fitting procedure. The fitted parameter α relates both to the Young's modulus and to the shape of the indenter. As $\delta F/\delta z_i = 2\alpha z_i$ (see Eqn 1) and:

$$\frac{\delta F}{\delta z_i} = \beta \frac{2}{\sqrt{\pi}} E_{\text{eff}} \sqrt{A} \quad (4)$$

(Oliver and Pharr, 2004), where the correction factor β may be approximated to 1 and A is calculated as shown in Fig. 1, the effective elastic modulus E_{eff} can be calculated:

$$\frac{\delta F}{\delta z_i} \approx \frac{2}{\sqrt{\pi}} E_{\text{eff}} 2 z_i \tan\theta = 2\alpha z_i$$

or

$$E_{\text{eff}} = \frac{\sqrt{\pi}}{2} \times \frac{\alpha}{\tan(\theta)} , \quad (5)$$

where θ is the tip angle of the indenter (35 deg. in our experiments). As described in Scholz et al. (Scholz et al., 2008), the Young's modulus may be calculated from E_{eff} if one knows the Poisson ratio of the sample. However, in the following, only the effective Young's modulus is calculated and depicted. The results of this calculation are given both as mean values with their standard deviations and as median values, as the data are not normally distributed.

The experiments were registered and approved by the local government (Landesamt für Natur, Umwelt und Verbraucherschutz Nordrhein-Westfalen) and performed according to the German law for animal care (AZ: 9.93.2.10.35.07.094).

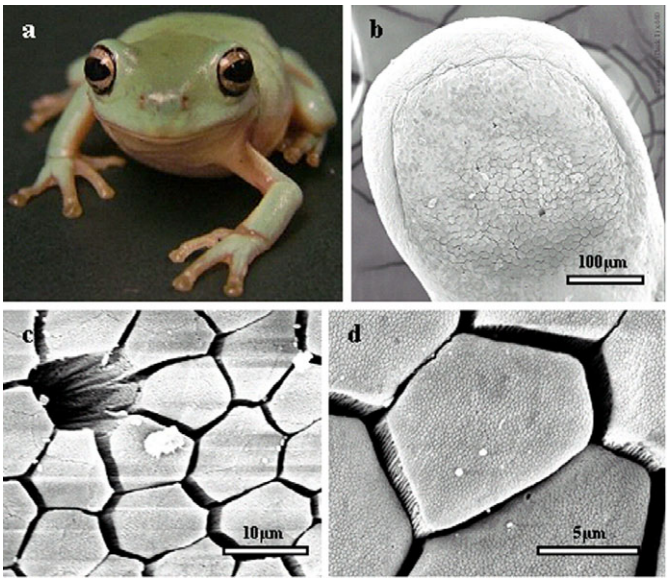

Fig. 2. (a) Immature White's tree frog, *Litoria caerulea* (snout–vent length, approximately 40 mm). (b–d) Scanning electron microscopy (SEM) of toe pad epithelium. (b) Low-power micrograph of whole pad of a juvenile frog. (c) Medium-power micrograph showing a mucous pore and (largely) hexagonal epithelial cells separated from each other at their distal ends by channels. (d) Higher power micrograph indicating the presence of nanostructuring on the 'flat' surface of the epithelial cells.

RESULTS

Toe pad ultrastructure in *Litoria caerulea*

As in other tree frogs, *Litoria caerulea* has large disc-like pads on the tip of each toe that aid adhesion (Fig. 2a). As can be seen from SEM studies, the epithelium of toe pads is specialised, and is delineated from normal skin epithelium by a number of grooves, of which the best developed in immature *Litoria* is the circumferal groove running around the top and sides of each toe pad (Fig. 2b). As the frog grows, two prominent grooves develop which separate each of the pads into a medial and two lateral parts (not shown). At higher power (Fig. 2c), the epithelial cells can be seen to be columnar, with flat tops separated from each other at their apices. Most are hexagonal but, as the figure shows, some are pentagonal and a few are heptagonal. Pores of mucous glands open into the channels between the epithelial cells (Fig. 2c). Toe pads thus possess an outer layer consisting of a hexagonal array of flat-topped cells separated by mucus-filled grooves, as in other tree frog species (Welsch et al., 1974; Green, 1979; McAllister and Channing, 1983; Green and Simon, 1986; Hertwig and Sinsch, 1995; Mizuhira, 2004).

Fig. 2d is the first to give any indication that the flat surface of the epithelial cells possesses its own nanostructures. In surface view (Fig. 3a) these appear as a tightly packed array of (mostly) hexagonal structures, each with a poorly defined central structure. At equivalent magnification, sections of the toe pad epithelium viewed under the TEM show both the deep channels that separate the epithelial cells at their apices and the closely packed columnar nanopillars (Fig. 3b). The latter are approximately as tall as they are broad, separated from one another by narrow clefts and filled with electron-dense material. In many species (the inset in Fig. 3b shows the hylid *Scinax ruber*) the nanopillars seem to form the ends of fibrils that run at right angles to the surface from deep in the cytoplasm, but this is not the case in immature *Litoria caerulea*.

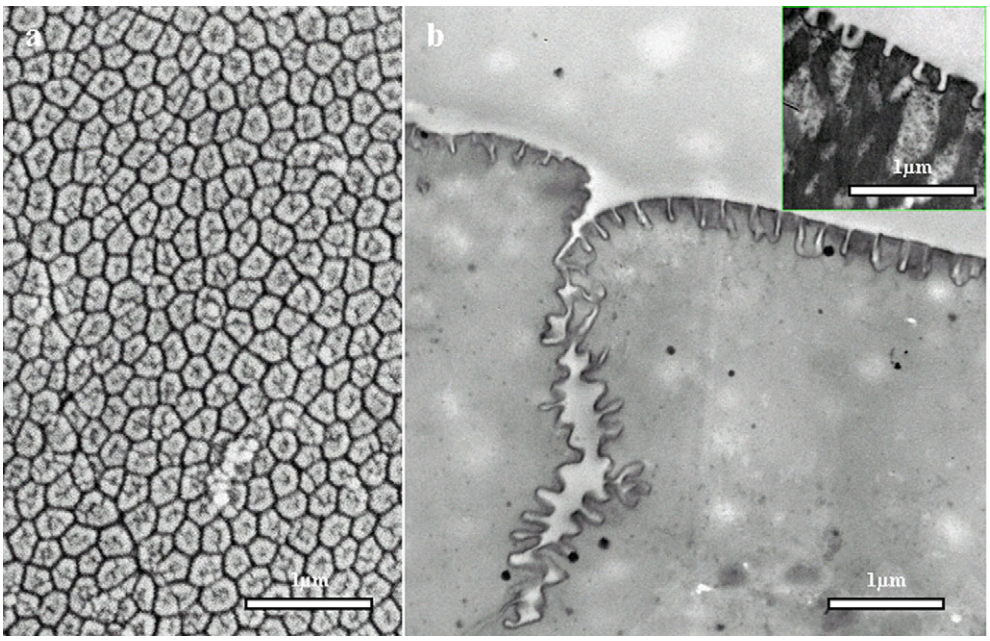

Fig. 3. (a,b) Nanostructural features of the adhesive surface of toe pad epithelial cells. (a) High-power scanning electron micrograph showing a surface view of the (largely) hexagonal nanostructures that form a dense array on the external surface of a toe pad epithelial cell. (b) High-power transmission electron micrograph showing one of the channels that separate adjacent epithelial cells and a side view of the nanostructures, which are themselves separated from each other by narrow channels. The inset shows similar nanostructures on a toe pad of the hylid tree frog, *Scinax ruber*. Here the nanostructures are associated with filaments running at right angles to the cell surface.

Freeze fracturing the toe pad tissue before viewing it under the SEM provides a side-on view of cytoskeletal elements within the toe pad epithelium (Fig. 4). The figure shows parts of two epithelial cells, their outer surfaces being at the top of the electron micrograph, while the channels between them and their neighbours are the U- or V-shaped structures at the top left, top centre-right and top right of the image. Cytoskeletal elements appear as a loose lattice or sponge-like structure. Conspicuously, the diameters of the pores of this structure are smaller towards the outer surface of the cell. The pores directly underneath the surface have diameters less than 0.5 µm and form the borders of the nanopillars. Within the underlying cytoplasm the diameters of the pores are larger (>1 µm), while in deeper layers there is just a loose lattice of cytoskeletal material. Therefore the concentration of cytoskeletal elements is higher at the outer surface of the epithelial cells in keeping with the TEM studies (Fig. 3b).

Atomic force microscopy (AFM)

As recognised by Scholz and colleagues (Scholz et al., 2008), the use of AFM has the advantage that it allows material properties to be analysed at a high spatial resolution, due to the small size of the pyramidal tip and the low forces of indentation. This makes it possible to examine the properties of the external adhesive surface independent of the mechanical arrangement of the adhesive pad as a whole. Additionally, and no less importantly, it analyses structure in living tissue, avoiding the shrinkage and deformation of structures that frequently results from tissue fixation. When applied to very soft tissues, as here, cantilever load is critical: too high and you 'plough' through the tissue damaging the cantilever; too low and you do not follow contours accurately. During indentation experiments, such problems also led to a number of occasions where the fit to the theoretical curve was poor, presumably because of cantilever damage. This was tested using 'goodness of fit' criteria as described previously (Baumgartner et al., 2000). Such data were excluded from the calculations of effective elastic modulus and resulted in gaps in our mapping of E_{eff} in different regions of the toe pads (Table 1). In spite of these difficulties, we have confidence in the results presented here. The nanostructural features seen using AFM match what we see using electron microscopy techniques too well for our AFM images to be artefacts, while force–distance curves derived from indentation experiments were an excellent match to theoretical curves for soft, elastic materials (Fig. 7a).

Typical AFM images and a 3D reconstruction of the surface topography are shown in Fig. 5. The AFM images broadly confirmed the morphological findings obtained by SEM and TEM. The images of the toe pad epithelial cells clearly show the rough surface of each cell and the deep channels that separate them. Furthermore, the deflection image (Fig. 5c) clearly shows the dense array of columnar nanopillars, referred to as peg-like hemidesmosomes by other authors (e.g. Ernst, 1973). However, the term hemidesmosomes is misleading as the structures observed clearly do not correspond to

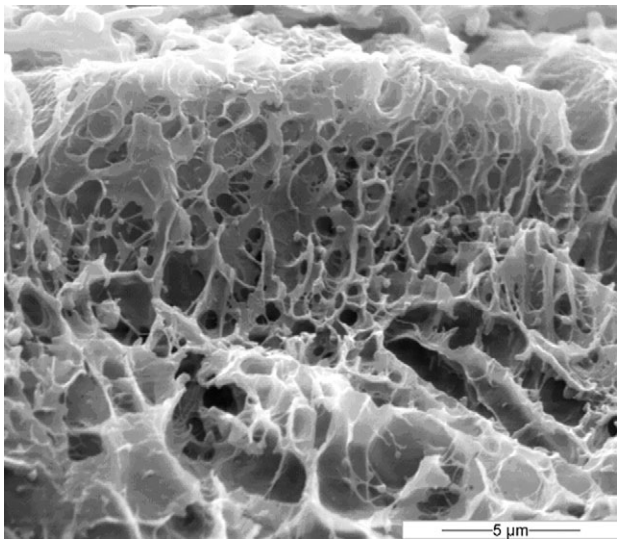

Fig. 4. Freeze-fracture image of a toe pad showing a side view of parts of two epithelial cells. Note that cytoskeletal elements are concentrated in the outer 'nanopillar' layer (top of picture), with only a loose lattice of cytoskeletal material beneath.

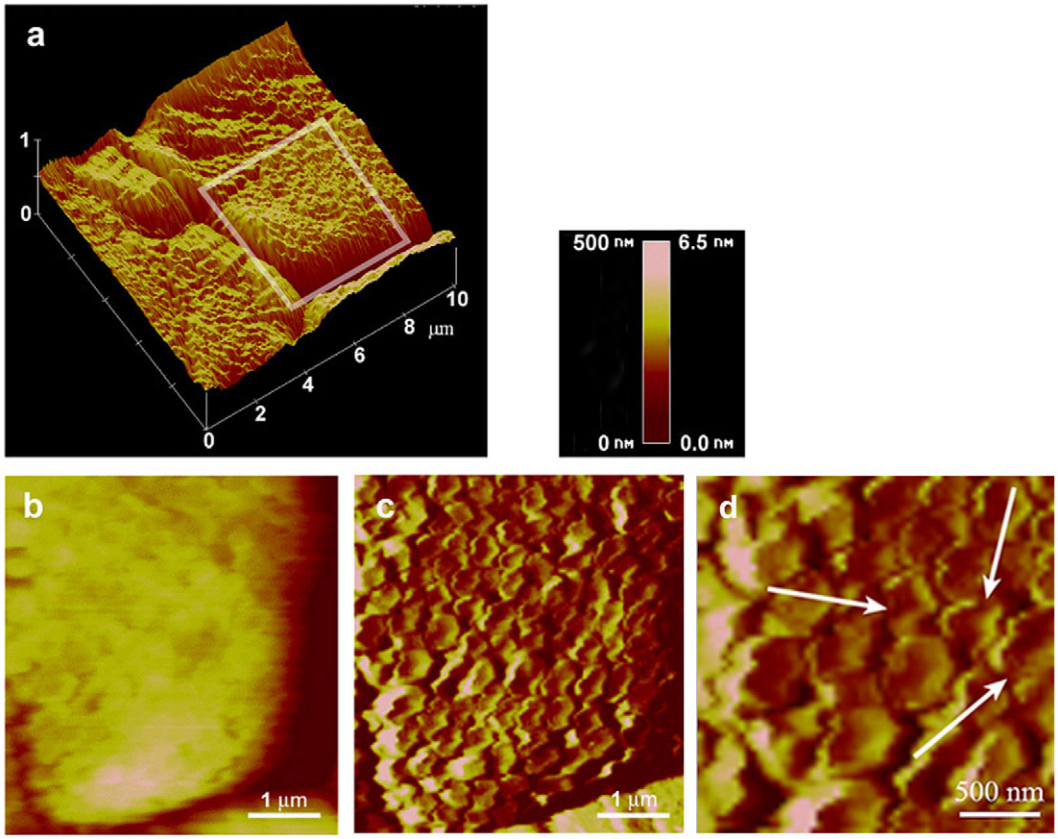

Fig. 5. (a) Three-dimensional reconstruction of the surfaces of parts of three toe pad epithelial cells, showing the rough surface of each cell and the deep channels that separate them. (b,c) AFM images (b, height and c, deflection) of part of one of these cells, indicated by the outline in a. The height image (of which b is a part) was used for the three-dimensional reconstruction (a), while the deflection image (c) clearly shows the dense array of peg-like nanopillars that constitutes the adhesive surface of the epithelial cells. (d) Enlargement of part of the deflection image showing more detail of the appearance of the nanopillars. The arrows indicate gaps connecting the dimples with the surrounding channels. For the height image (b), the colour gradient covers the range 0–500 nm, while for the deflection images (c and d) the range is 0–6.5 nm.

the cell organelles of that name that bind epithelial cells to the basement lamina (e.g. Alberts et al., 2002). The topography was consistent in all frogs observed and throughout the adhesive organ. Neither changing the scanning direction nor varying the scanning force significantly changed the principal structure. However, the width of the nanopillars was increased by increasing the scanning force from about 2 to 30 nN from a value of 313.8±78 to 409.9±76.7 nm (P<0.001; d.f.=188; t-test; measurements from four scans, all from the same toe pad). This indicates a rather soft material for these nanopillars. Interestingly, the AFM images illustrated a feature of the nanopillars not clearly visible in fixed tissue. This was the presence of a depression or 'dimple' on the top of each nanopillar. Close examination of these dimples in deflection images indicated that the wall surrounding the dimple was not continuous but had one or two channels connecting the dimple with the surrounding space between the nanopillars. These are indicated by the arrows in Fig. 5d.

Table 1. Measuring the stiffness of tree frog toe pad epithelium

Frog no.	Position	N	α (nN nm^{-2})	E_{Eff} (MPa)
1	Distal	10	$2.7\times10^{-5}\pm2.6\times10^{-6}$	0.03±0.003
1	Middle	10	$4.5\times10^{-3}\pm8.0\times10^{-4}$	5.70±1.01
1	Proximal	10	$4.8\times10^{-4}\pm2.3\times10^{-5}$	0.61±0.03
2	Proximal	10	$2.0\times10^{-2}\pm7.0\times10^{-3}$	25.32±8.86
2	Middle	12	$6.5\times10^{-3}\pm2.0\times10^{-3}$	8.23±2.53
3	Proximal	15	$1.3\times10^{-2}\pm9.6\times10^{-3}$	16.46±12.15
3	Proximal	17	$1.8\times10^{-3}\pm4.0\times10^{-4}$	2.28±0.51
3	Middle	14	$5.2\times10^{-2}\pm4.6\times10^{-2}$	65.83±58.24
3	Distal	14	$4.3\times10^{-3}\pm1.4\times10^{-3}$	5.44±1.77

Estimates of Young's modulus of elasticity (effective elastic modulus E_{Eff}; means ± s.d.) from atomic force microscopy. Multiple measurements on three subadult *Litoria caerulea* from different positions on the toe pads. Overall mean is 14.4±20.9 MPa and median 5.7 MPa. α, material parameter related to Young's modulus.

To analyse the nanopillars further, height profiles were calculated from the topography data. A typical example of such a profile is depicted in Fig. 6. Nanopillars with an average width of about 326 nm can be clearly seen to possess a central shallow depression (dimple), about 8 nm in depth. Making these measurements on 199 nanopillars (seven scans including the four described in the previous paragraph; scanning forces were 2 nN and 30 nN) yielded an average width for the nanopillars of 326±84 nm, which is comparable to the data obtained by SEM and TEM, and an average depth of the central dimple on the nanopillars of 7.7±4.2 nm. The heights of the nanopillars were also measured (21.4±8.4 nm), but are not included in the figure as they seriously underestimate the height of the structures as seen under TEM (Fig. 3b). Presumably the tip of the AFM cantilever was unable to penetrate the narrow channels between the nanopillars effectively. Indeed, given the dimensions of the AFM cantilever, it can be calculated that its tip would only be able to penetrate the channels to a depth of about 18 nm, assuming the channel width of 25 nm estimated by Federle and colleagues (Federle et al., 2006).

In order to quantify the mechanical parameters of the frogs' adhesive pads, we performed indentation experiments by recording force–distance measurements with the AFM. A typical force–distance cycle is depicted in Fig. 7a. As a control, all cantilevers used were initially tested on a glass plate. The corresponding force–distance curve is shown in Fig. 7b. The curves show characteristic and reproducible shapes. While for the

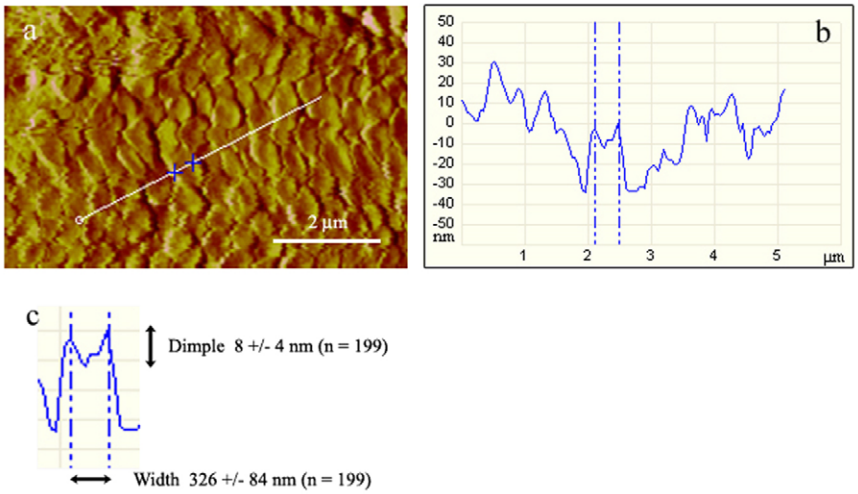

Fig. 6. (a–c) Height profiling of toe pad epithelium. (a) Deflection image showing the line from which the height profile (b) was taken. The two crosses delineate a columnar nanopillar that lay precisely on the profile line, showing that these peg-like structures have a small dimple at their centres. (c) Average values (means ± s.d.) of the width of the nanopillars and the depth of the dimples based on 199 measurements from height profiles such as that shown in b.

glass substrate, representing a hard material, the deflection increases almost immediately after the tip has touched the surface with a slope of 1, the curve obtained on the frog adhesive pad clearly shows a different behaviour. After the tip has touched the surface, the deflection starts slowly, indicating that the *z*-movement of the piezo-actuator is mainly transferred to indentation of the soft pad material. Then the slope of the curve continuously increases as, because of the pyramidal form of the tip, the pad material resistance increases while the spring constant of the cantilever stays constant. The green lines in the figures show the theoretical fits of the data according to the theoretical behaviour described in Materials and methods. As discussed above, the fits are very good, indicating that the assumptions of ideal indentation of a pyramidal tip in a homogeneous thick material are well fulfilled. Repetitive measurements did not reveal any significant plastic deformations (not shown), i.e. the pad material was not influenced by viscous effects or plastic deformation but behaves primarily elastically under the loads applied during the measurements. The existence of a small hysteresis between indentation and recovery components of the force–distance cycles does, however, indicate a degree of viscoelasticity. The fits of the force–distance cycles allow the determination of the parameter α that is related to the tip geometry and the effective Young's modulus E_{eff}. The α and E_{eff} values are given in Table 1. Although the absolute values of E_{eff} showed significant variation over three orders of magnitude, some variation is to be expected. The cytoskeletal thickening of the cell surface is uneven, with considerable variation in thickness from one region to the next (Fig. 5). Because of the presence of the cytoskeleton, the pad surface is a 'fibre reinforced material' where the value of E_{eff} depends on whether pure matrix material or a fibre track is indented. Also, the surface of a pad is not flat, and differences due to placement of the tip of the indenter with respect to the nanopillars would also be expected. However, as we were careful not to make indentations near the edges of the epithelial cells, influences from the deep channels between the cells can be excluded. We failed to find any significant differences between different animals or between different positions on the pad, though results for the latter are sparser than we would have wished for the reasons discussed above. The basic results were, however, consistent with the conclusion that the toe pad epithelium is a soft and elastic material with an effective elastic modulus that has a mean value of 14 MPa (median value 5.7 MPa). By combining Eqns 1 and 5, it is possible to calculate δz_i for different values of E_{eff}. For a force change of 30 nN, δz_i is 195 nm for an E_{eff} of 1 MPa and 62 nm for an E_{eff} of 10 MPa. Since such a force change increased the diameter of nanopillars by about 100 nm as described above, the median estimate of E_{eff} is at least approximately verified if one assumes that the volume of the nanopillars remains constant (increase in width is 36 nm for an E_{eff} of 10 MPa and 192 nm for an E_{eff} of 1 MPa if nanopillar retains its cylindrical shape). Such calculations can also be applied to the range of values for E_{eff} found here. In our scans, local height changes in the pad surface (excluding channels between nanopillars) could exceed 150 nm. The above calculation shows that such variation would be produced by E_{eff} changes of one

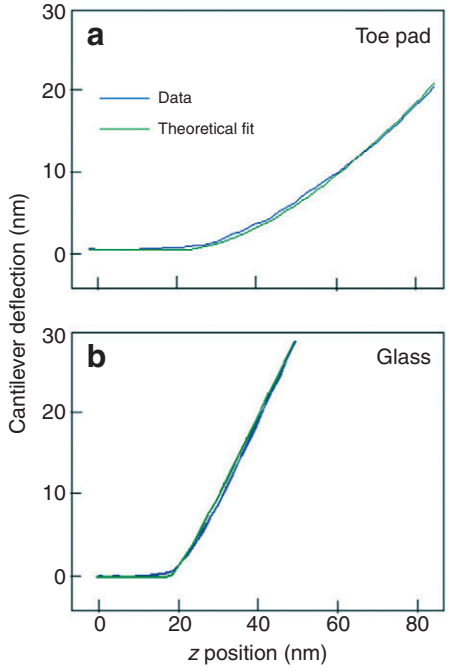

Fig. 7. Material stiffness as measured by the AFM. (a,b) Blue lines show typical experimental curves for cantilever deflection plotted against distance in the *z*-axis for toe pad epithelium (a) and glass (b). Green lines are fits to the best theoretical curves using Eqn 3. The *y*-axes can be converted to force by multiplying by the spring constant of the cantilever (0.03 N m^{-1} in these experiments). The curve in a represents an effective elastic modulus E_{eff} of 250 kPa.

order of magnitude, and is compatible with our data (Table 1) if we exclude the two extreme outliers (frog 1 distal and frog 3 middle). Without these values, the mean E_{eff} is reduced to 9.1±8.7 MPa, while the median is unchanged.

DISCUSSION

Requirements for adhesion and friction

As tree frog toe pads have evolved as structures that can produce friction and adhesion forces sufficient to permit climbing and reduce the risk of falling, their micro- and ultra-structural features must be considered as adaptations for these functions.

All natural surfaces are to some degree rough, and this roughness occurs at many different length scales (Persson et al., 2005). Such materials do not adhere, because the interaction between neutral molecules is negligibly small at separations of the order of only a few atomic distances and the roughness prevents close enough contact between the surfaces (Kendall, 2001). To get over this problem, at least one of the surfaces must be extremely soft, so that the softer material conforming to the contours of the other can increase actual contact. Additionally, the presence of fluid in the contact zone can fill out any remaining cavities, thus further increasing adhesion (Federle, 2006).

Turning to friction, the presence of a continuous fluid film in the contact zone would normally be expected to act as a lubricant. The existence of significant friction forces in tree frog toe pads is thus somewhat surprising. Indeed, whole animal measurements of adhesion and friction indicate that friction forces are about 1.5 times greater than adhesive ones (Barnes et al., 2006b). Persson (Persson, 2007) calculates that areas separated by low viscosity fluid [as is the case in tree frogs (Federle et al., 2006)] with a thickness of more than a few nanometres will contribute a negligible friction force. It must therefore be presumed that there is actual contact between the two surfaces at many places. This is supported by the existence of static friction between pad and substrate and frictional forces remaining 2 min after movement has ceased (Federle et al., 2006). Indeed, Federle and colleagues (Federle et al., 2006) demonstrate, using interference reflection microscopy, that pad–substrate distances over the central regions of the hexagonal epithelial cells in living, adhering tree frogs range from 0 to 35 nm. Thus, combining wet adhesion and good friction requires the pad surface to be highly structured, so that both wet adhesion produced by fluid in the contact zone and friction through direct pad–substrate contact can occur simultaneously.

Roles for toe pad microstructures

In functional terms, having the cells separated at their tips reduces the bending modulus of the pad epithelium, which allows the pads to conform to the shape of large-scale irregularities (greater in area than the flat surfaces of individual epithelial cells) on the surface to which the frog is adhering (Barnes, 1999; Barnes et al., 2002; Persson, 2007). The mucous glands are required to produce the watery secretion that forms an essential part of the adhesive mechanism of the pad, while the hexagonal array of channels that surround each epithelial cell presumably functions to spread mucus evenly over the pad surface and, under wet conditions, remove surplus water (Barnes et al., 2002; Persson, 2007). Finally, the presence of grooves aids adhesion by reduction of crack propagation (peeling) (Persson, 2007). Pull-off stress is spread between a larger number of hexagons rather than being concentrated at the edge of the contact zone. Such features have been incorporated into bio-inspired artificially patterned surfaces to increase their adhesion (for a review, see Barnes, 2007b).

A common misconception is that the subdivision of the surface by the channels between the cells increases adhesion according to the principle of contact splitting. This theory states that adhesive force is proportional to the length of the contact; therefore, by splitting up the contact zone into many small areas of contact, the total adhesive force can be increased in direct proportion to the density of these small areas (Arzt et al., 2003). This principle clearly applies to wet adhesion (De Souza et al., 2008). However, as the major force component of wet adhesion is capillarity, it is necessary that an air–water interface (meniscus) should surround each small area of contact. This is true of the hairy pads of insects (Federle, 2006), but not of tree frogs, where the meniscus surrounds the whole toe pad, not the individual epithelial cells (Federle et al., 2006).

AFM and nanostructural features of toe pad epithelial cells

The AFM results provide further insights into the detailed characteristics of the nanoscale topography of the toe pad epithelial cells as well as demonstrating that their surface is soft (effective elastic modulus of 14.4±20.9 MPa, equivalent to silicon rubber).

The functions of the nanopillars that constitute the so-called ‘flat’ surface of these cells remain a matter for speculation. The following is a list of obvious possibilities, none of which are mutually exclusive. (1) Like the epithelial cells and the channels that surround them, the nanopillar array may allow close conformation to surface irregularities, but on a much smaller length scale (nanometres rather than micrometres) than applies to whole epithelial cells; such close conformation is promoted both by the presence of the grooves surrounding each nanopillar and by the softness (low effective elastic modulus) of the surface material. Additionally, the nanopillars make the pad softer (than the pure material) due to their bending. (2) The narrow channels between them could serve to absorb excess water, much as sipes (fine-scale grooves) do on a wet-weather car tyre (see Persson, 2007). This would allow rapid optimisation of the thickness of the intervening fluid layer (as thin as possible, but without any air pockets). (3) The nanopillars could be very important in the generation of friction forces, in that their tips will be in actual contact with the surface. This would explain the presence of static friction and other phenomena that are seen when recording friction forces from single toe pads (Federle et al., 2006). Interestingly, interference reflection microscopy of tree frog toe pads during tilting experiments shows friction-induced reductions in the thickness of the fluid layer, the toe pads coming into closer contact with the substrate as the angle of tilt changes from 0 to 90 deg. As a result, more and more nanopillar tips come into contact with the glass coverslip (J.M.S., M. O. Riehle, W.J.P.B. and J. R. Downie, in preparation). Increased friction thus appears to be directly linked to increases in nanopillar–substrate contact. (4) It cannot be excluded that the dimples give rise to a suction effect, but the existence of channels in the dimple wall makes this unlikely. Indeed, it is more likely that the channels allow the escape of fluid from the dimples when the pad is pressed against a smooth surface, thus minimising fluid layer thickness and increasing close contact of nanopillars with the surface.

Significance of low effective elastic modulus (E_{eff})

In an earlier study, Barnes and colleagues (Barnes et al., 2005) examined the physical properties of the toe pads of *Litoria* using a spherical indenter, with indentation depths in the range 50–350 μm. They came up with values for E_{eff} of between 4 kPa and 20 kPa, much lower than most of the values obtained here. E_{eff} is thus inversely dependent on the indentation depth. This is reflected by the TEM and freeze-fracture images, which indicate cytoskeletal

strengthening of the plasmalemma. Having a higher concentration of cytoskeleton elements near the surface of the pad also seems to be one of the facts that influence the high variation of E_{eff}. Both variations in the thickness of the elements and especially their sponge-like arrangement result in significant changes in stiffness for different indentation positions. Overall, this construction leads to a thin but slightly harder 'skin', with a Young's modulus equivalent to silicon rubber, covering a soft gel-like structure, the cytosol of the epithelial cells where there are relatively few ctyoskeletal elements. Blood sinuses lie more centrally (J.M.S. and W.J.P.B., unpublished observation). This might provide an abrasion-resistant surface layer that, due to the soft tissue and fluids lying beneath, would have enough flexibility to cope with surface roughness as discussed above. Such a 'design' contrasts with smooth adhesive pads in stick insects, which have evolved an extremely soft outer layer (the epicuticle) overlying a much stiffer procuticle (Scholz et al., 2008).

Biomimetic relevance

Since adhesive tapes inspired by the dry adhesive mechanisms of gecko toe pad setae are now reaching a stage where commercialisation is imminent (e.g. Lee et al., 2007; Lee et al., 2008; Schubert et al., 2008), it is appropriate to consider whether the rather different wet adhesion mechanism of tree frogs might also have biomimetic relevance. An obvious possibility is the development of improved wet weather tyres (Barnes, 1999; Barnes et al., 2002; Persson, 2007). Tree frog toe pads have an effective elastic modulus akin to rubber that surrounds a much softer material. They also have three systems of grooves at different length scales. The similarities to wet weather tyres are uncanny, and their performance (easy detachment combined with high coefficient of friction) impressive. But whether tree frog adhesive mechanisms can operate effectively when scaled up by two orders of magnitude remains to be tested. Biomedical applications of these findings are also under consideration.

LIST OF ABBREVIATIONS

A	area of AFM indenter tip at indentation depth (z_i)
AFM	atomic force microscope/microscopy
d	AFM cantilever deflection
E_{eff}	effective elastic modulus
F	applied force
m	exponent representing geometry of AFM indenter
SEM	scanning electron microscope/microscopy
TEM	transmission electron microscope/microscopy
w	width of AFM indenter tip at indentation depth (z_i)
z	vertical position of AFM piezo drive
z_i	indentation depth
z_0	zero position of AFM piezo drive (tip touching surface)
α	material parameter related to Young's modulus
β	correction factor (see Oliver and Pharr, 2004)
θ	tip angle of AFM indenter

W.J.P.B. and J.M.S. would like to thank The Wellcome Trust for their financial support of this project (Showcase Award; Grant No. 070924) and Dr Walter Federle for the opportunity to carry out the freeze-fracture studies in his laboratory in Würzburg. Deposited in PMC for release after 6 months.

REFERENCES

Alberts, B., Johnson, A., Lewis, J., Raff, M., Roberts, K. and Walter, P. (2002). *Molecular Biology of the Cell.* New York: Garland Science.
Arzt, E., Gorb, S. and Spolenak, R. (2003). From micro to nano contacts in biological attachment devices. *Proc. Natl. Acad. Sci. USA* **100**, 10603-10606.
Autumn, K. and Peattie, A. M. (2002). Mechanisms of adhesion in geckos. *Integr. Comp. Biol.* **42**, 1081-1090.
Autumn, K., Dittmore, A., Santos, D., Spenko, M. and Cotkosky, M. (2006). Frictional adhesion: a new angle on gecko attachment. *J. Exp. Biol.* **209**, 3569-3579.
Barnes, W. J. P. (1999). Tree frogs and tire technology. *Tire Technol. Int.* **March 1999**, 42-47.
Barnes, W. J. P. (2006). Dynamic adhesion in animals: mechanisms and biomimetic implications. *J. Comp. Physiol. A* **192**, 1165-1168.
Barnes, W. J. P. (2007a). Functional morphology and design constraints of smooth adhesive pads. *MRS Bull.* **32**, 479-485.
Barnes, W. J. P. (2007b). Biomimetic solutions to sticky problems. *Science* **318**, 203-204.
Barnes, W. J. P., Smith, J., Oines, C. and Mundl, R. (2002). Bionics and wet grip. *Tire Technol. Int.* **December 2002**, 56-60.
Barnes, W. J. P., Perez-Goodwyn, P. and Gorb, S. N. (2005). Mechanical properties of the toe pads of the tree frog, *Litoria caerulea*. *Comp. Biochem. Physiol. A*, **141**, S145.
Barnes, W. J. P., Federle, W. and Drechsler, P. (2006a). Adhesion and friction forces generated by single toe pads of the frog *Litoria caerulea*. *Comp. Biochem. Physiol. A* **143**, S94.
Barnes, W. J. P., Oines, C. and Smith, J. M. (2006b). Whole animal measurements of shear and adhesive forces in adult tree frogs: insights into underlying mechanisms of adhesion obtained from studying the effects of size and shape. *J. Comp. Physiol. A* **192**, 1179-1191.
Barnes, W. J. P., Pearman, J. and Platter, J. (2008). Application of peeling theory to tree frog adhesion, a biological system with biomimetic implications. *Eur. Acad. Sci. E Newsl. Sci. Technol.* **2008**, **1**, 1-2.
Baumgartner, W., Hinterdorfer, P. and Schindler, H. (2000). Data analysis of interaction forces measured with the atomic force microscope. *Ultramicroscopy* **82**, 85-95.
De Souza, E. J., Brinkmann, M., Arzt, E. and Mohrdieck, C. (2008). Enhancement of capillary forces by multiple liquid bridges. *Langmuir* **24**, 8813-8820.
Duellman, W. and Trueb, L. (1997). *Biology of Amphibians. 2*nd edn. Baltimore, MD: Johns Hopkins University Press.
Emerson, S. B. and Diehl, D. (1980). Toe pad morphology and mechanisms of sticking in frogs. *Biol. J. Linn. Soc.* **13**, 199-216.
Ernst, V. (1973). The digital pads of the tree frog, *Hyla cinerea*. 1. The epidermis. *Tissue Cell* **5**, 83-96.
Federle, W. (2006). Why are so many adhesive pads hairy? *J. Exp. Biol.* **209**, 2611-2621.
Federle, W., Barnes, W. J. P., Baumgartner, W., Drechsler, P. and Smith, J. M. (2006). Wet but not slippery: boundary friction in tree frog adhesive toe pads. *J. R. Soc. Interface* **3**, 589-601.
Gorb, S. and Scherge, M. (2000). Biological microtribology: anisotropy in frictional forces of orthopteran attachment pads reflects the ultrastructure of a highly deformable material. *Proc. R. Soc. Lond. B* **267**, 1239-1244.
Green, D. M. (1979). Treefrog toe pads: comparative surface morphology using scanning electron microscopy. *Can. J. Zool.* **57**, 2033-2046.
Green, D. M. (1981). Adhesion and the toe-pads of tree frogs. *Copeia* **1981**, 790-796.
Green, D. M. and Simon, P. (1986). Digital microstructure in ecologically diverse microhylid frogs genera *Cophixalus* and *Sphenophryne* (Amphibia: Anura) from Papua New Guinea. *Aust. J. Zool.* **34**, 135-145.
Hanna, G. and Barnes, W. J. P. (1991). Adhesion and detachment of the toe pads of tree frogs. *J. Exp. Biol.* **155**, 103-125.
Hertwig, I. and Sinsch, U. (1995). Comparative toe pad morphology in marsupial frogs (genus *Gastrotheca*): arboreal versus ground-dwelling species. *Copeia* **1995**, 38-47.
Kendall, K. (2001). *Molecular Adhesion and its Applications.* New York: Klewer.
Lee, H., Lee, B. P. and Messersmith, P. B. (2007). A reversible wet/dry adhesive inspired by mussels and geckos. *Nature* **448**, 338-341.
Lee, J., Majidi, C., Schubert, B. and Fearing, R. S. (2008). Sliding-induced adhesion of stiff polymer microfibre arrays. I. Macroscale behaviour. *J. R. Soc. Interface* **5**, 835-844.
McAllister, A. and Channing, L. (1983). Comparisons of toe pads of some Southern African climbing frogs. *S. Afr. J. Zool.* **18**, 110-114.
Mizuhira, V. (2004). The digital pads of rhacophorid tree-frogs. *J. Electron Microsc. (Tokyo)* **53**, 63-78.
Morris, V. J., Kirby, A. R. and Gunning, A. P. (1999). *Atomic Force Microscopy for Biologists*. London: Imperial College Press.
Oliver, W. C. and Pharr, G. M. (2004). Measurement of hardness and elastic modulus by instrumented indentation: advances in understanding and refinements to methodology. *J. Mater. Res.* **19**, 3-20.
Persson, B. N. J. (2007). Wet adhesion with application to tree frog adhesive toe pads and tires. *J. Phys. Condens. Matter* **19**, 376110.
Persson, B. N. J., Albohr, O., Tartaglino, U., Volokitin, A. I. and Tosatti, E. (2005). On the nature of surface roughness with application to contact mechanics, sealing, rubber friction and adhesion. *J. Phys. Condens. Matter* **17**, R1-R62.
Scherge, M. and Gorb, S. (2001). *Biological Micro- and Nanotribilogy: Nature's Solutions.* Heidelberg: Springer Verlag.
Scholz, I., Baumgartner, W. and Federle, W. (2008). Micromechanics of smooth adhesive organs in stick insects: pads are mechanically anisotropic and softer towards the adhesive surface. *J. Comp. Physiol. A* **194**, 373-384.
Schubert, B., Lee, J., Majidi, C. and Fearing, R. S. (2008). Sliding-induced adhesion of stiff polymer microfibre arrays. I. Microscale behaviour. *J. R. Soc. Interface* **5**, 835-844..
Welsch, U., Storch, V. and Fuchs, W. (1974). The fine structure of the digital pads of Rhacophorid tree frogs. *Cell Tissue Res.* **148**, 407-416.